

## Approximate Minimum-Time Trajectories for 2-link Flexible Manipulators

G.R. Eisler, D.J. Segalman, R.D. Robinett<sup>†</sup>  
*Sandia National Laboratories, Albuquerque, New Mexico*

### Abstract

Powell's nonlinear programming code, VF02AD, has been used to generate approximate minimum-time tip trajectories for 2-link semi-rigid and flexible manipulator movements in the horizontal plane. The manipulator is modeled with an efficient finite-element scheme for an n-link, m-joint system with horizontal-plane bending only. Constraints on the trajectory include boundary conditions on position and energy for a rest-to-rest maneuver, straight-line tracking between boundary positions, and motor torque limits. Trajectory comparisons utilize a change in the link stiffness,  $EI$ , to transition from the semi-rigid to flexible case. Results show the level of compliance necessary to excite significant modal behavior. Quiescence of the final configuration is examined with the finite-element model.

### Introduction

Trajectory planning is essential in budgeting a manipulator's actuator efforts to maximize productivity. For repetitive tasks, the minimum-time maneuver goes hand-in-hand with this goal. A variety of approaches have been advanced for rigid manipulator control, taking advantage of the fact that all or some of the controls take the form of switching functions between actuator bounds. Bobrow [1] used an intuitive approach to generate optimal switching controls, as well as proving the boundedness of the controls. Weinreb and Meier [2][3] used calculus of variations approaches to incorporate control bounds in the problem formulation. In a second study, Bobrow [4] used numerical optimization to generate spline fits to the switching controls.

Switching functions do not lend themselves to maintaining tip accuracy for non-rigid structures. One would hope that the applied controls do take advantage of the bounds to maximize performance, but a clear analytical directive for this does not exist at the present.

In filling this void, parameter optimization techniques can provide approximate optimal performance solutions for systems driven by complex, highly nonlinear dynamic models with arbitrary equality or inequality constraints. Of these solution techniques, Powell's Recursive Quadratic Programming algorithm [5], embodied in the code VF02AD, has proven to be a robust tool for a variety of aerospace applications [6][7][8], and will be used in this study. The primary drawback to this or other numerical optimization methods is the dependancy on accurate gradient approximations of the performance index and constraints with respect to the parameters.

The ensuing discussion initially describes the structural dynamics model of the manipulator, followed by the optimal control problem and parameterization of the controls, and ends with the results of a computational experiment.

The manipulator structure modeled in this study, and presently under fabrication, is a 2-link cantilever arrangement constrained to slew in the horizontal plane. Tall, thin links are used to

---

<sup>†</sup>Members of the Technical Staff, Engineering Analysis Department

minimize vertical plane droop. The hub or joint-1 actuator slews both links, an interlink motor, and tip payload. The interlink or joint-2 actuator located at the end of link-1 slews the second link and the tip payload. The joint-1/joint-2 actuator torque ratio is about 4/1. The complete manipulator is about 0.5 meters (m) tall and 1.2m long.

### **The Structural Model**

There is a long literature discussing the difficulties of simulating the vibrations of rotating structures[9] [10] [11]. The problem seems to arise from kinematics that are of second order importance in nonrotating problems, but become of first order importance in the presence of rotational accelerations. Additionally, there are constraints inherent to the flexible link problem which must be satisfied: motions occur entirely in a horizontal plane; one end of the chain of links is attached to a stationary hub; and each flexible link is inextensible. These considerations motivate the development of a mathematical model that faithfully carries the full kinematics of the problem. It is also necessary to devise such a model in a form that will lend itself to real-time calculations.

The need to meet these apparently conflicting demands motivated the development of a model specialized to flexible, multilink structures. That apparently successful strategy is outlined below. The full kinematics are retained by expressing the configuration as functions of convected coordinates. This is a traditional approach in nonlinear elasticity [12]. Further, the kinematic variables are selected so that all geometric constraints (fixed hub, planar motion, and non-extension) are automatically satisfied.

Since motions are assumed to occur entirely in a plane, it is also assumed that the elastic lines of the links as well as the mass centers of the cross sections all lie in the same plane. Each cross section is identified by its arc-length distance from the hub, so that the orientation of the center of the cross section  $s$  at time  $t$  is

$$\vec{\beta}(s, t) = \cos(\theta(s, t))\vec{i} + \sin(\theta(s, t))\vec{j}$$

The location of the center of cross section  $s$  at time  $t$  is obtained by integration of the above unit tangent vector:

$$\vec{x}(s, t) = \int_0^s \vec{\beta}(s', t) ds'$$

Similarly, the velocity at the cross section  $s$  at time  $t$  is obtained by integration of the time derivative of  $\vec{\beta}(s, t)$ :

$$\dot{\vec{x}}(s, t) = \int_0^s \dot{\theta}(s', t)\vec{\gamma}(s', t) ds'$$

where

$$\vec{\gamma}(s, t) = -\sin(\theta(s, t))\vec{i} + \cos(\theta(s, t))\vec{j}$$

The above description of configuration - entirely in terms of  $\theta(s, t)$  - causes all of the geometrical constraints to be satisfied automatically. Additionally, the above description expresses the configuration in terms of one unknown field ( $\theta$ ), instead of the more conventional two or three fields ( $x$ ,  $y$ , &  $\theta$ ).

The governing equations of the dynamics are derived using those kinematics and a frame-invariant variational method - Hamilton's principle. A finite element discretization is used to cast the resulting integro-differential equations for  $\theta(s, t)$  and its first and second derivatives into a system of fully-coupled, nonlinear algebraic equations. Particularly important for the application at hand is the observation that since all spatial integrals are with respect to the convected coordinate,  $s$ , those integrals are configuration-independent and need be done only once. The nonlinearities

remain, and a new nonlinear system must be solved at each time step, but the time consuming quadrature process can be done in advance of the dynamics simulation. These features are illuminated below through derivation.

Hamilton's principle is that

$$\delta \int_{t_1}^{t_2} [KE(t') - SE(t') + WE(t')] dt' = 0 \quad (1)$$

where  $KE$  is kinetic energy,  $SE$  is strain energy, and  $WE$  is external work. Quantities associated with the end times,  $t_1$  and  $t_2$  have to do with initial and final conditions and the conservation of momenta, but the governing equations necessary to model motion of the flexible structure are obtained by consideration of the integrand alone:

$$\delta KE(t) - \delta SE(t) + \delta WE(t) = 0 \quad (2)$$

for all  $t_1 \leq t \leq t_2$ .

The kinetic energy is that of the flexible links plus that of all concentrated masses and concentrated moments of inertia:

$$KE(t) = \frac{1}{2} \int_0^L \rho(s) \dot{\vec{x}}(s, t) \cdot \dot{\vec{x}}(s, t) ds + \frac{1}{2} \sum_{k=1}^{masses} M_k \dot{\vec{x}}(s_k, t) \cdot \dot{\vec{x}}(s_k, t) + \frac{1}{2} \sum_{l=1}^{inertias} I_l \dot{\theta}(s_l, t) \cdot \dot{\theta}(s_l, t)$$

The strain energy is that of the flexible links:

$$SE(t) = \frac{1}{2} \int_0^L \kappa(s) \frac{\partial \vec{\beta}(s, t)}{\partial s} \cdot \frac{\partial \vec{\beta}(s, t)}{\partial s} ds$$

Discretization of the above energy terms is obtained by discretizing the tangent vector  $\vec{\beta}$  as:

$$\vec{\beta}(s, t) = \sum_{n=1}^{nodes} \vec{\beta}_n(t) p_n(s)$$

where the shape functions,  $p_n$ , have support over intervals that are small relative to the anticipated radii of curvature. The above condition on the support of the basis functions is necessary to assure compliance with the condition of nonextension. The resulting energies are:

$$KE(t) = \frac{1}{2} \sum_{m=1}^{nodes} \sum_{n=1}^{nodes} \dot{\theta}_m(t) \dot{\theta}_n(t) \vec{\gamma}_m(t) \cdot \vec{\gamma}_n(t) M_{m,n} \quad (3)$$

and

$$SE(t) = \frac{1}{2} \sum_{m=1}^{nodes} \sum_{n=1}^{nodes} \vec{\beta}_m(t) \cdot \vec{\beta}_n(t) K_{m,n} \quad (4)$$

where

$$M_{m,n} = \int_0^L \rho(s) q_m(s) q_n(s) ds + \sum_{k=1}^{masses} M_k q_m(s_k) q_n(s_k) + \sum_{l=1}^{inertias} I_l \delta_K(l, m) \delta_K(l, n),$$

$$q_m(s) = \int_0^s p_m(\hat{s}) d\hat{s}, \quad K_{m,n} = \int_0^L \kappa(s) p'_m(s) p'_n(s) ds,$$

$\delta_K$  is the Kronecker delta function,  $\hat{s}$  is a dummy variable, and  $p'_{m,n}$  are spatial derivatives.

After appropriate integration by parts, the integrand of equation 2 becomes:

$$\sum_{n=1}^{nodes} \delta\theta_m (-\vec{\gamma}_m(t) \cdot \ddot{\vec{\beta}}_n(t) M_{m,n} - \vec{\gamma}_m(t) \cdot \vec{\beta}_n(t) K_{m,n} + \vec{\gamma}_m(t) \cdot \vec{\tau}_n(t) \delta_K(m, n)) = 0 \quad (5)$$

for all nodes  $m$ . In the above equation,  $\tau_n$  is the external torque applied at node  $n$ . After  $\ddot{\vec{\beta}}_n(t)$  is expanded:

$$\ddot{\vec{\beta}}_n(t) = \ddot{\theta}_n(t) \vec{\gamma}_n(t) + (\dot{\theta}_n(t))^2 \vec{\beta}_n(t)$$

and Equation 5 is invoked for all  $\delta\theta_m$ , a complete set of *nodes* second order equations in the *nodes* unknowns,  $\ddot{\theta}_n$ , results as follows:

$$\sum_{n=1}^{nodes} \vec{\gamma}_m(t) \cdot \vec{\gamma}_n(t) \ddot{\theta}_n(t) M_{m,n} - \vec{\gamma}_m(t) \cdot \vec{\beta}_n(t) (\dot{\theta}_n(t))^2 M_{m,n} + \vec{\gamma}_m(t) \cdot \vec{\beta}_n(t) K_{m,n} = \vec{\gamma}_m(t) \cdot \vec{\tau}_m(t) \quad (6)$$

The above problem formulation, involving only one unknown field, automatically satisfying all constraints, and requiring only one evaluation of element mass and stiffness matrices, lends itself to rapid numerical calculation. A computer code to generate and solve the above described system of equations for each time step has been written, tested and used by VF02AD. Both the derivation and code mentioned above are described more fully in Ref. [13].

One particularly interesting calculation, discussed in the literature as being difficult to solve, is that of a beam accelerated around a hub to an angular frequency above the first bending frequency of the beam. This is a particularly stringent test of flexible-dynamics codes, testing numerical robustness, as well as the correctness of the physics. Figure 1 shows the motion of the tip of such a flexible beam relative to the tip of a rigid beam rotating at the hub velocity. Initially, the flexible beam lags its rigid counterpart; it then overtakes and oscillates about the rigid beam. These results are in near exact agreement with the results presented in [9], obtained from a much more complex model.

### Optimal Trajectory Shaping

The principle goal in this study is to combine the physics of the structure with optimization techniques to generate actuator torque histories for accomplishing a useful task with minimal degradation in performance. A secondary objective is to shortcut the work of an eventual feedback controller, which will be needed to compensate for modeling errors.

Looking towards maximizing productivity in some repetitive task, a minimum-time tip trajectory was chosen for investigation. Constraints on such a trajectory include: completing a rest-to-rest maneuver, tracking a specified path  $(x(t), y(t))_{tip}$ , slewing between specified endpoints  $[(x(t_o), y(t_o)), (x(t_f), y(t_f))]_{tip}$ , and not exceeding actuator torque limits  $\tau_{1,2,max}$ .

The configuration initially starts at rest. Driving a flexible structure to rest at the final time,  $t_f$ , necessitates end constraints on both kinetic and potential or strain energies  $(KE(t_f), SE(t_f))$ . The chosen path is a straight line and actuator torques limits are constants. The problem can be



sample trajectories.

ITEM	COMPOSITION	LENGTH (m)	MASS (kg)	STIFFNESS, $EI$ (newton-m <sup>2</sup> )
joint-1 bracket	1 element	.0635	.545	$10^5$
link-1	3 elements	.5040	.640	$10^2, 10^3$
1st joint-2 bracket + joint-2	1 element + 1 point mass	.1070	5.415	$10^5$
2nd joint-2 bracket	1 element	.1040	.830	$10^5$
link 2	3 elements	.4890	.313	$10^2, 10^3$
Totals:	9 elements	1.2675	7.743	

The two values of stiffness,  $EI$ , for links 1,2 represent the trajectory comparison for this study. The brackets, modeled with a stiffness of  $10^5$ , are considered rigid. Point moments of inertia were used to define mass distribution for the brackets. No payload was used in this comparison. The joints were assumed to have no compliance or damping.

The two trajectories, computed on a CRAY-XMP, were integrated for 100 time steps, where  $\Delta t = .01t_f$ . Trajectory evaluations for gradient computations executed in 0.75 secs. The torque histories for each joint were composed of 21 tabular values, where  $\Delta \zeta = .05$ . Torque bounds were chosen as  $\pm 16, \pm 4$  newton-m (n-m) for joints 1 and 2. The path to be tracked for this study was the line connecting  $(x, y)$  pairs,  $(0.0, 1.13)$  and  $(1.13, 0.0)$ . A composite of the slew motion for the "flexible" case ( $EI_{links} = 100$  newtons-m<sup>2</sup>) is given in Fig.2. The parameterized torque histories that created this slew represent 100 iterations of VF02AD after initialization with the parameter solution values from the "semi-rigid" case ( $EI_{links} = 1000$  n-m<sup>2</sup>). The tip path traced is reasonably straight, but does contain some small ripples - a result of the integral statement of the tracking constraint,  $C_3(t_f)$ .

Figure 3 graphically depicts the difference between the semi-rigid and flexible links. Shown is the angular velocity of the finite-element node adjacent to joint 1. The frequency of vibration for  $EI_{links} = 100$  is about 19 hz. From examination of Fast Fourier transforms (FFTs) of the finite-element output of the system disturbed about the initial, midtime, and final positions, this appears to be one of the lower modes. Note the low angular velocity of the semi-rigid system after  $t/t_f = 0.9$ , implying that a significant amount of time is being expended in order to bring the system to "rest". This phenomena is definitely at odds with purely rigid system behavior. The  $KE(t_f) = 0$  constraint imposes a zero final angular velocity in both cases. Also, note that  $t_f$  for the flexible case is slightly greater than the semi-rigid one. This demonstrates the approximate nature of the solutions, insofar as the semi-rigid solution not converging as well.

Fig.4 shows the  $\tau_1$  profiles. These still retain some of the boundedness qualities of purely rigid configurations. However, they begin and end near zero instead of the bounds ( $\pm 16$  n-m), and the transition between bounds is comparatively gradual. The oscillatory behavior in the  $EI_{links} = 100$  torque is probably counteracting the excitement of the lowest structural modes, which would have the greatest impact on the position constraints. Note the abruptness of the controls near the end in an attempt to quiet the structure. The  $\tau_2$  torques in Fig.5 show minimal activity for most of the trajectory, except close to the end in order to accomplish the rest state. Note that this closing maneuver starts sooner with the more flexible link structure.

The straight-line tracking error in millimeters (mm) is shown in Fig.6. Both torque histories appear to limit the error to  $\pm 5$  mm except near the end of the  $EI_{links} = 1000$  trajectory, where the error momentarily "escapes" before returning to zero to satisfy the end position constraints,  $(C_1(t_f), C_2(t_f))$ . One drawback to the integral formulation is that it can relax tracking performance in isolated parts of the trajectory, yet yield a reasonably low residual ( $\approx 0$ ) for  $C_3(t_f)$ . It may be

necessary to add interior point constraints to significantly decrease this error. A less complex alternative is to reduce the  $EI_{links}$  more gradually between solutions, in the fashion of a homotopy scheme, until the desired value is reached.

The kinetic energy of the flexible structure at peak rates ( $t/t_f \approx 0.45$ ) is, not surprisingly, higher than the semi-rigid one as shown in Fig.7. It is interesting that  $KE$  appears to be devoid of oscillatory behavior in both cases. Note again, the rest phase of the trajectories above  $t/t_f = 0.9$ . Strain energy is shown in Fig.8. This again displays the contrast first seen in Fig.3. The semi-rigid structure produces relatively little strain, while the flexible-link configuration again contains the 19 hz mode with a sizable increase in energy magnitude. Note the peaks in both cases, mirroring the sharp  $\tau_1$  changes in Fig.4. Also, note the enforcement of the  $SE(t_f) = 0$  point constraint at the end. The  $SE$  "floor" in both cases corresponds to the  $KE$  peaks in Fig.7.

The finite-element model was also able to examine the quiescence of the final state. At  $t_f$ , joint node accelerations can be zeroed and joint node positions fixed at their nominal final values. The corresponding torques applied to maintain these values can then be computed. Fig.9 shows the residual  $\tau_1$  being applied after the approximate optimal  $t_f = 1.505$  secs for  $EI_{links} = 100$  has been reached. The oscillations in this residual appear to contain frequencies in the vicinity of 2.5 and 35 hz. The lower appears to correspond to a fixed-free mode of the first link with the remainder of the system mass concentrated at the end. This mode was not seen during the optimized part of this trajectory. The second frequency may be a higher harmonic of the mode seen earlier, or possibly a numerical artifact. The small magnitude of this residual coupled with the spacing of the modes may be ideal targets for attack by a linear feedback control scheme. As an open-loop alternative, augmenting the tabular torque controls with frequency-based, parameterized functionals may be sufficient to suppress these oscillations.

## Conclusions

A robust, parameter optimization tool has been able to generate actuator torque histories for approximate, minimum-time slewing maneuvers containing a variety of continuous and point constraints for a 2-link flexible manipulator. The parameters, or actuator torques, for each link were tabular values at fixed node points during the maneuver. Perturbations were made to each parameter to approximate final time and constraint gradients. The efficient formulation of the finite-element model made the numerical optimization procedure a realistic endeavor.

The accuracy of the straight-line tip tracking was good. Additional interior constraints and/or a more gradual change in the stiffness should yield further improvements. For the trajectory used in this study, joint-1 applied most of the input, which included cancelling lower-mode vibrations for the structural as a whole. Energy constraints were effective in bringing the structure to rest at  $t_f$ . It was also demonstrated that final energy constraints do not preclude vibrations during the slew. The intended production use of the manipulator will dictate whether this is a hindrance or not. Finally, the secondary goal of providing enough vibration control to maximize the success of a linear feedback controller in treating residual oscillations appears feasible.

## References

- [1] J.E. Bobrow, S. Dubowksy and J.S. Gibson, "Time-Optimal Control of Robotic Manipulators along Specified Paths", *Int. J. Robotics Res.*, Vol 4.,no.3, Fall 1985.
- [2] Weinreb, A., Bryson, A.E., "Optimal Control of Systems with Hard Control Bounds", *IEEE Transactions on Automatic Control*, Vol.AC-30, No.11, Nov. 1985, pp.1135-1138.

- [3] E.B. Meier and A.E. Bryson, "An efficient algorithm for time-optimal control of a two-link manipulator," in AIAA conference on Guidance, Navigation, and Control, Monterey, CA, Aug 1987, pp 204-212.
- [4] Bobrow, J.E., "Optimal Robot Path Planning Using the Minimum-Time Criterion", *IEEE J. Robotics and Automation*, Vol.4, No.4, August 1988.
- [5] Powell, M.J.D., "A Fast Algorithm for Nonlinearly Constrained Optimization Calculations", *Proceedings of the Biennial Conference on Numerical Analysis*, Springer-Verlag, Berlin, 1978, pp.144-157.
- [6] Eisler, G.R., Hull, D.G., "Maximum Terminal Velocity Turns at Nearly Constant Altitude", *Journal of Guidance, Control, and Dynamics*, Vol.11, No.2, March-April 1988, pp.131-136.
- [7] Outka, D.E., "Parameter Optimization Capability in the Trajectory Code PMAST", SAND86-2917, Sandia National Laboratories, Albuquerque, 1987.
- [8] Robinett, R.D., "A Unified Approach to Vehicle Design, Control, and Flight Path Optimization", The Center for Strategic Technology, Texas A&M University, SS87-1, 1987.
- [9] J. C. Simo and L. Vu-Quoc 'The role of non-linear theories in transient dynamic analysis of flexible structures', *Journal of Sound and Vibration*, Vol. 119, 1987, pp 487-508.
- [10] T. R. Kane, R. R. Ryan, and A. K. Banerjee, 'Dynamics of a cantilever beam attached to a moving base', *Journal of Guidance, Control and Dynamics*, Vol. 10, 1987, pp 139-151.
- [11] S. Hanagud and S. Sarkar, 'Problem of the dynamics of a cantilever beam attached to a moving base', *Journal of Guidance, Control and Dynamics*, Vol. 12, 1989, pp 438-441.
- [12] A. E. Green and W. Zerna, *Theoretical Elasticity*, Clarendon Press, Oxford, 1954.
- [13] D. J. Segalman, 'A Mathematical Formulation for the Rapid Simulation of a Flexible Multilink Manipulator' SAND89-2308, Sandia National Laboratories, Albuquerque, New Mexico.

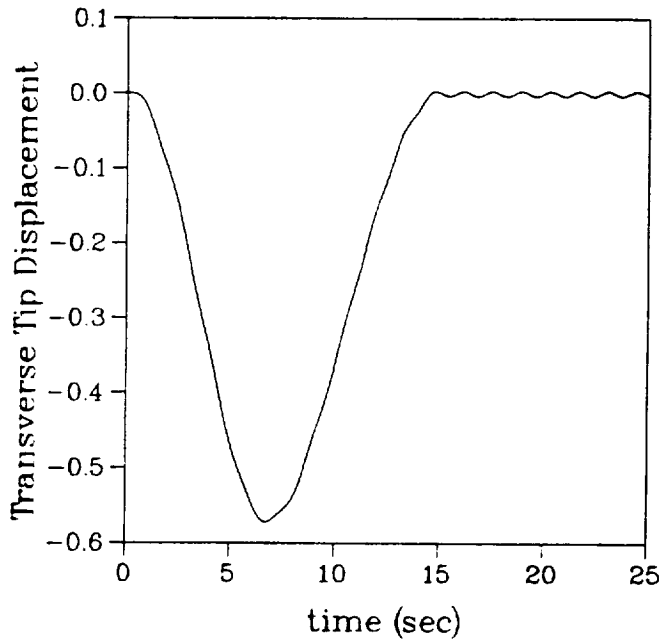


Figure 1: Single beam relative tip motion

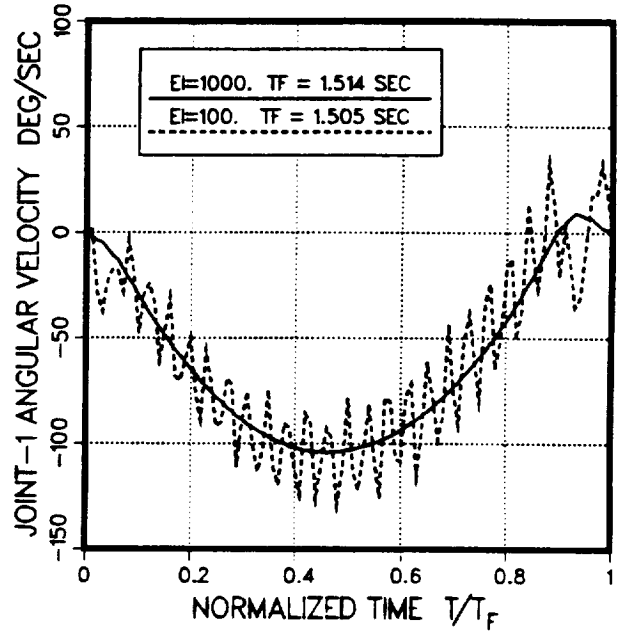


Figure 3: Joint 1 node angular velocity

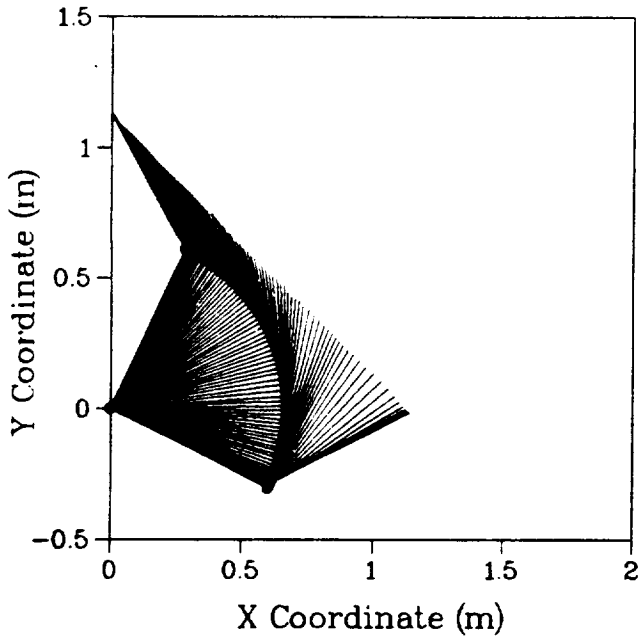


Figure 2: Composite motion for  $EI_{links} = 100$

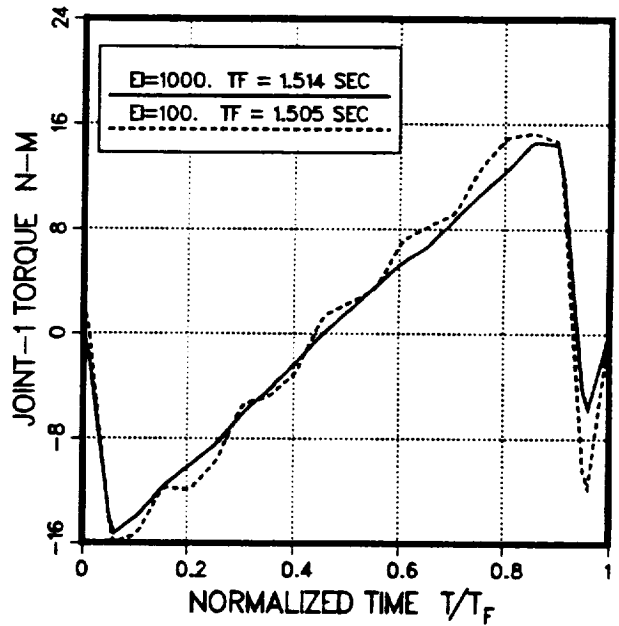


Figure 4:  $\tau_1$  joint torque histories

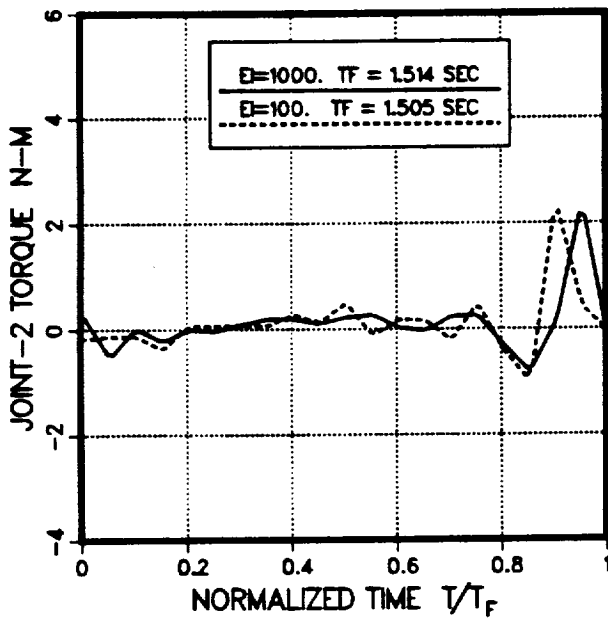


Figure 5:  $\tau_2$  joint torque histories

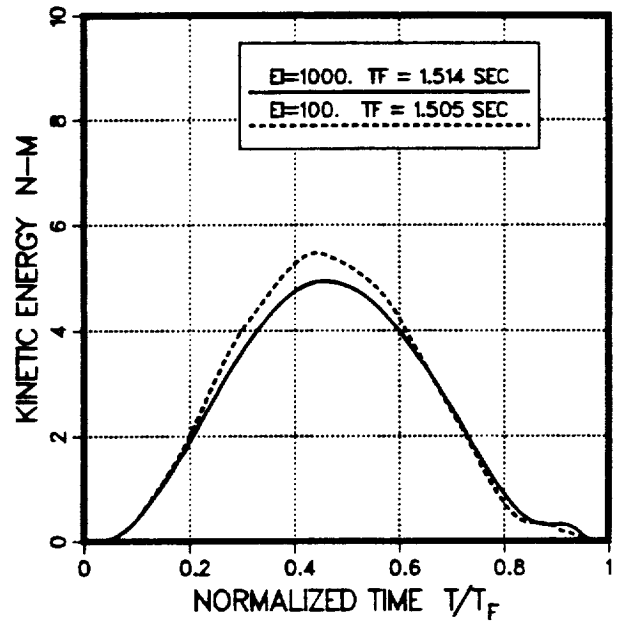


Figure 7: Kinetic energy histories

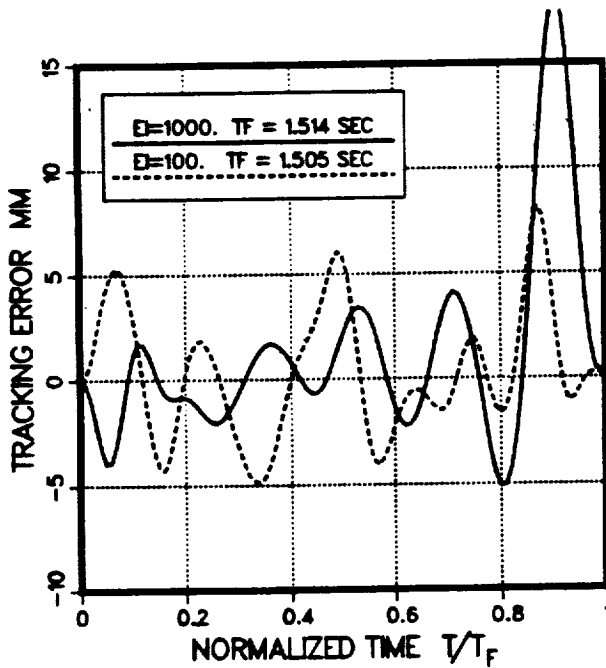


Figure 6: Straight-line tracking error

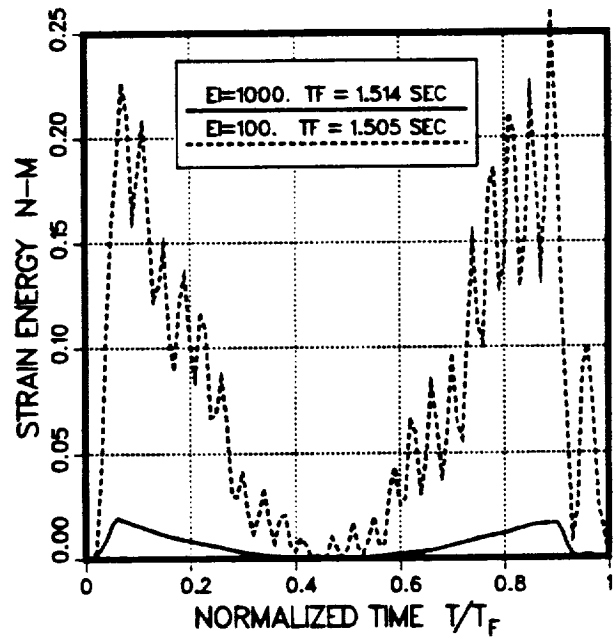


Figure 8: Strain energy histories

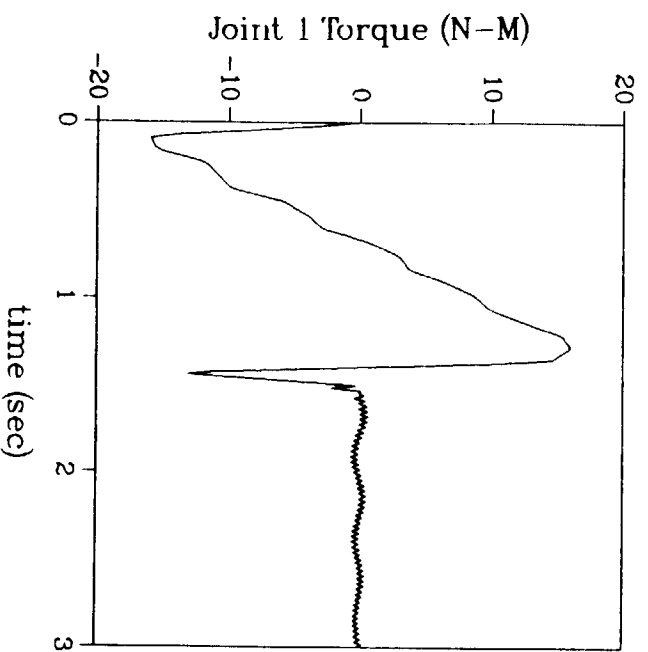


Figure 9: Residual  $\tau_1$  for  $EI_{link_1} = 100$